Available online at www.sciencedirect.com
ScienceDirect
Journal of Hazardous Materials 152 (2008) 690–698
Journal of Hazardous Materials
www.elsevier.com/locate/jhazmat

Hybrid surfactant-templated mesoporous silica formed in ethanol and its application for heavy metal removal

Hong Yang [a], Ran Xu [a], Xiaoming Xue [a], Fengting Li [a,*], Guangtao Li [b]

[a] *State Key Lab of Pollution Control and Resource Reuse Study, College of Environmental Science and Engineering, Tongji University, 200092 Shanghai, China*
[b] *Department of Chemistry, Tsinghua University, 100084 Beijing, China*

Received 9 February 2007; received in revised form 28 June 2007; accepted 12 July 2007
Available online 25 July 2007

Abstract

With cetyltrimethylammonium (CTAB) and tetramethylammonium hydroxide (TMAOH) as hybrid surfactant templates, a mesoporous adsorbent (adsorbent C) was synthesized in ethanol via the integration of "One-step" procedure and "Evaporation-Induced Self-Assembly" procedure. During the synthesis, TMAOH served as the subsidiary structure-directing agent. Adsorbent C exhibited higher pore diameter (centered at 6.1 nm), BET surface area (421.9 m^2/g) and pore volume (0.556 cm^3/g) than the other two adsorbents only using P123 (adsorbent A) or CTAB (adsorbent B) as the surfactant. The adsorbents were also characterized by XRD and FTIR spectroscopy. The adsorption of copper, zinc, lead, iron, silver and manganese ions on adsorbent C was investigated by contrast tests with adsorbent A and B. The experimental data showed that adsorbent C possessed better adsorption properties than the counterparts. The order of adsorption capacity for six metal ions was $Mn^{2+} < Zn^{2+} < Cu^{2+} < Fe^{2+} < Pb^{2+} < Ag^{+}$. The kinetic and thermodynamic properties and the regeneration capacity of adsorbent C were also discussed.

Keywords: Mesoporous silica; Heavy metal removal; Adsorbent; Tetramethylammonium hydroxide; Evaporation-induced self-assembly

1. Introduction

A large variety of heavy metals are discharged to the environment, causing serious environmental pollution and threatening people's health, even at low concentrations. At the same time, many of them (e.g. silver, lead and copper) are precious and can be recycled and reused for extensive applications. Therefore, the removal and recovery of the heavy metals from wastewater are attracting more and more attention from the public for both ecological and economic benefits. The adsorption technology is one of the most popular methods to control such pollutants. Numerous adsorbents have been surging in recent years, such as mesoporous materials functionalized with various organic groups [1–3].

Many mesoporous materials possess excellent adsorption capacity, due to their large surface area, ordered pore arrangement, uniform pore sizes and controllable modifying ratio of functional groups. Although the expense for mesoporous adsorbents per unit is relatively high, some of them have been proved to be economical by regeneration experiments, in which the adsorbents maintained the great adsorption capacity for heavy metals after multiple repeated uses [4,5].

"Hydrothermal-synthesis" process is a common method to prepare mesoporous materials [6,7]. This method requires organic and inorganic reactants combining in the water phase, which easily results in faster hydrolysis of organosilane and reduces the cross-linking degree of organosilane and silica framework as well as intake of functional groups. "Evaporation-Induced Self-Assembly" (EISA) procedure is based on sol–gel chemistry and mainly used for preparation of mesoporous films [8–12]. "EISA" chooses organic solvent as reaction media, which can make up the deficiency of traditional "hydrothermal-synthesis" process. Under the condition of acid catalysis, silica source is pre-hydrolyzed with added water in organic solvents. Simultaneously, the surfactant is dispersed in the solvent to form supramolecular structure. Then the above solutions are mixed to guarantee the interactivity between surfactants and silica. Due to the evaporation of the organic solvent, the concentration of surfactant gradually increases. When it exceeds the critical micelle concentration (CMC), micelles will form in the solution.

* Corresponding author. Tel.: +86 21 65983302; fax: +86 21 65983121.
E-mail address: fengting@mail.tongji.edu.cn (F. Li).

0304-3894/$ – see front matter © 2007 Elsevier B.V. All rights reserved.
doi:10.1016/j.jhazmat.2007.07.060

Subsequently, the co-self-assembly of micelles and silica leads to the formation of mesophase and the achievement of mesoporous, crystalline materials [13–16]. "EISA" helps to efficiently control the hydrolysis and cross-linking rates of organosilanes. Mesostructure is induced during the solvent evaporation, as a result, higher modifying ratio of functional groups can be obtained, which easily leads to the comparatively smaller pore size [17]. The common solvents used in synthesis of mesoporous materials are toluene [18], methanol [19] and tetrahydrofuran [20]. However, all these solvents have high toxicity and are harmful to the environment. It is necessary to reduce the toxicity of solvents even choose nontoxic ones.

Meanwhile, "Two-step" procedure (namely post-synthesis treatment), is to graft organic groups onto the performed mesopore channel surface [21–23], which easily leads to the morphology destruction [24] and low ratio of modified functional groups [25]. In comparison, "One-step" procedure is to directly incorporate organic groups into silica frame by co-condensation [26], which can result in an uniform distribution of functional groups inside the mesopore channels but leads to smaller pore size [27–29].

According to the synthesis methods of mesoporous materials reported, TMAOH is a common component used for not only providing an alkali environment for the synthesis of mesoporous materials, but also serving as an auxiliary template. J. Perez-Pariente et al. [30] reported the thiol-MCM-41 samples obtained by TMAOH and surfactants possessed a surface area higher than synthesized by the standard preparation. Li and coworkers [31] synthesized the Ti-MCM-41 from gel using TMAOH as the auxiliary template. The XRD pattern indicated the molecular sieve had higher crystallinity using TMAOH than $NH_3{\cdot}H_2O$. Proper $TMAOH/SiO_2$ ratio (0.27) availed the formation of the long-range-ordered structure, which meant a wormhole framework with an increased length of mesopore channels [32]. In addition, TMAOH played an important role in the pore size expansion process [33,34]. Therefore, the utilization of TMAOH in the synthesis of the mesoporous materials can solve the problem of small pore size produced in both "One-step" and "EISA" procedure.

A new approach for preparing mesoporous adsorbents was provided in this study, which was using TMAOH as the subsidiary structure-directing agent and nontoxic ethanol as the organic solvent, and combining "One-step" and "EISA" procedure to fabricate the mesoporous adsorbent. The adsorption of copper, zinc, lead, iron, silver and manganese ions on the obtained adsorbent was investigated by contrast tests with two adsorbents synthesized using a conventional procedure [35]. In addition, its kinetic and thermodynamic properties were discussed.

2. Experimental

2.1. Reagents and materials

3-Aminopropyltriethoxysilane (APTES, 99%) and a triblock copolymer (Pluronic P123, $EO_{20}PO_{70}EO_{20}$, Mav = 5800) were purchased from Aldrich. Tetraethyl orthosilicate (TEOS), cetyltrimethylammonium (CTAB), absolute ethyl alcohol, $NaHCO_3$ and HCl (36 wt.%) were purchased from Shanghai Chemical Co. and tetramethylammonium hydroxide (TMAOH, 25 wt.%) was provided by Zhenfeng Chemical Co. All the above materials were used without further purification. Nitrates of copper, zinc, lead, iron, silver and manganese were used to prepare metal ion solution. No further pH adjustment of these solutions was made since hydrolysis of metals prevented the precipitation of the corresponding metal hydroxides. Deionized water was used throughout this work.

2.2. Instruments

FTIR spectra were obtained from a Spectrum 2000 FTIR spectrometer (Perkin-Elmer) with the usual KBr pellet method. X-ray diffraction (XRD) test were performed on a Rigaku D/max-RB diffractometer with CuK_α radiation. Nitrogen adsorption tests were performed at 77 K using a Coulter Omnisorp 100 gas analyzer. The concentrations of Cu^{2+}, Zn^{2+}, Pb^{2+}, Fe^{2+}, Ag^{+} and Mn^{2+} remaining in the solutions were analyzed by an Inductively Coupled Plasma Spectrometer (ICP, Optima 2100 DV, America) after appropriate dilution. The pH values were measured by a pH-meter (PHS-3C, China).

2.3. Synthesis of mesoporous adsorbents

2.3.1. Synthesis of adsorbent A using P123 as surfactant

A typical synthetic procedure used APTES, TEOS, P123, HCl, H_2O and ethanol in relative molar ratios of 0.25:1:0.022:0.025:6.25:40.76. Four grams of P123 was dissolved in 40 g dry ethanol and vigorously stirred for 2 h. Meanwhile, 1.76 g APTES, 0.4 g HCl (2 mol/L), 3.6 g H_2O and 20 g dry ethanol were mixed and also stirred for 2 h. Then 6.64 g TEOS was slowly added into the mixture of the above two solutions. The mixture was stirred for further 1 h. After reaction, the product was transferred into a Petri dish for solvent evaporation at room temperature. The resulting solid was aged in deionized water at 90 °C for 3 d. After recovered by filtration, the solid product was refluxed in ethanol/HCl for 1 d at 70 °C to extract the surfactant templates. Then it was filtered, stirred in 1 mol/L $NaHCO_3$ solution overnight and washed with deionized water for neutralization. Finally, it was dried under vacuum at 60 °C for 1 d to obtain powder adsorbent.

2.3.2. Synthesis of adsorbent B using CTAB as surfactant

A procedure similar to which described above was followed, except that 2.19 g CTAB replaced 4 g P123 as surfactant. The molar composition of the reaction mixture, APTES:TEOS:CTAB:HCl:H_2O:ethanol, was 0.25:1:0.188:0.025:6.25:40.76.

2.3.3. Synthesis of adsorbent C using CTAB as surfactant and TMAOH as subsidiary structure-directing agent

A procedure similar to which described above was followed, except that 2.19 g CTAB replaced 4 g P123 as surfactant, 3.6 g TMAOH solution (25 wt%) replaced 3.6 g H_2O as subsidiary structure-directing agent. The molar composition of the reaction

mixture, APTES:TEOS:CTAB:HCl:TMAOH:H_2O:ethanol, was 0.25:1:0.188:0.025:0.309:4.69:40.76.

2.4. Adsorption test

Metal nitrates were dissolved in deionized water to prepare initial metal ion solutions with different concentrations. In a typical run, 0.05 g of adsorbent and 10 mL of metal ion solution were placed in stoppered vials and sonicated for 20 min at room temperature. The resulting mixture was filtered through a 0.45 μm Uniflo filter unit and the filtrate was analyzed via ICP/OES spectroscopy. The loading capacity for a given metal ion was then calculated by the change in concentration between the filtrate and the initial metal ion solution.

2.5. Adsorption kinetics test

Fifty milligrams of adsorbent C and 10 mL of 1 mmol/L Cu^{2+} solution were placed in stoppered vials and sonicated for 1, 2, 3, 4, 5, 10, 15, 20 min at room temperature. The resulting mixture was filtered through a 0.45 μm Uniflo filter unit and the filtrate was analyzed via ICP/OES spectroscopy.

2.6. Cycle use of adsorbent C

The samples loading Cu^{2+} were used to verify the regeneration capacity. In a typical run, 0.1 g of adsorbent C and 20 mL of 1 mmol/L Cu^{2+} solution were placed in stoppered vials and sonicated for 20 min at room temperature. The resulting mixture was filtered through a 0.45 μm Uniflo filter unit and the filtrate was analyzed via ICP/OES spectroscopy. Then the copper-loaded adsorbent was placed in 100 mL of 1 mol/L HCl, stirred for 4 h to elute metal ions at room temperature. After filtration, the adsorbent was neutralized with 1 mol/L $NaHCO_3$ solution for 12 h, washed with deionized water and used again. Following another filtration, adsorbent C was dried in a vacuum oven at 60 °C before another use.

2.7. Adsorption isotherm test

Metal nitrates were dissolved in deionized water to prepare initial metal ion solutions with concentrations of 0.5 mmol/L, 1 mmol/L, 2 mmol/L and 4 mmol/L. Fifty milligrams of adsorbent C and 10 mL of metal ion solution were placed in stoppered vials and sonicated for 20 min at room temperature. The resulting mixture was filtered through a 0.45 μm Uniflo filter unit and the filtrate was analyzed via ICP/OES spectroscopy.

3. Results and discussion

3.1. Preparation and characterization

TEOS and APTES were used as silica sources and TEOS/APTES ratio of 4 was used to promote the formation of better morphologic structures and the increase of modified functional ligands [36]. The synthesis procedure is shown in Fig. 1. Using nontoxic ethanol as the only organic solvent, APTES

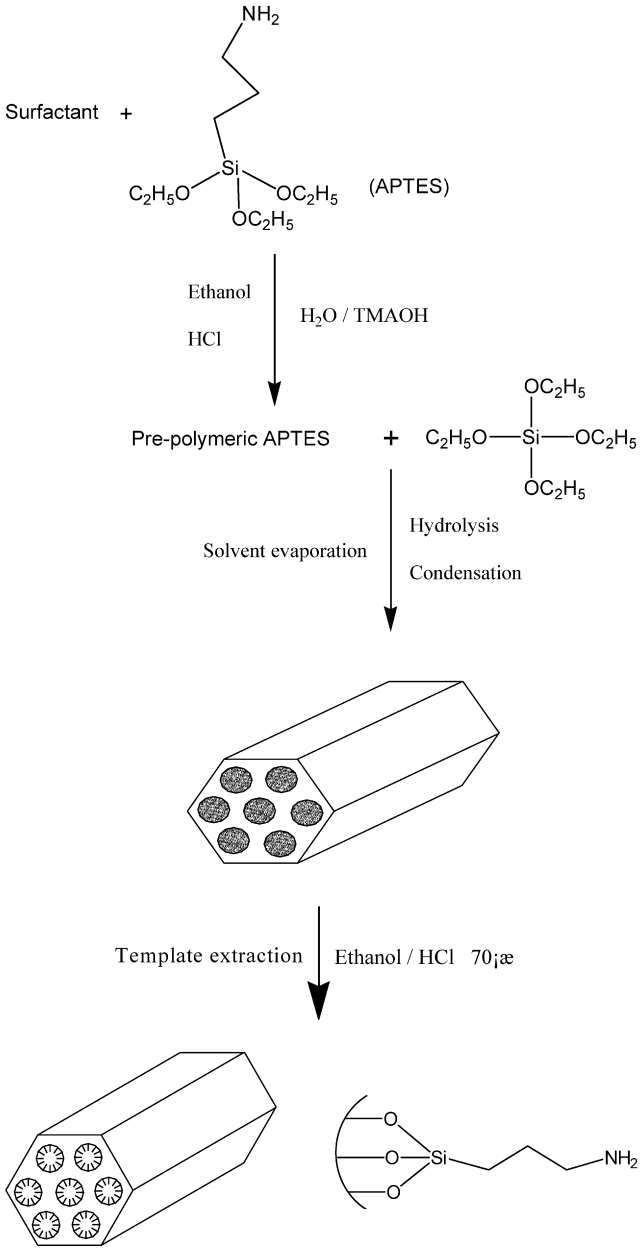

Fig. 1. The schematic synthesis route of three mesoporous adsorbents.

was slowly hydrolyzed and pre-polymerized with the surfactant micelle. Then pre-polymeric APTES and the hydrolyzate of added TEOS were partically co-condensed by Si–OH. During the evaporation of ethanol, the silica were further hydrolyzed and cross-linked to form ordered mesostructures.

Three adsorbents were characterized by FTIR to ascertain the modification of $-NH_2$. The FTIR patterns present similar location and appearance of the major bands in Fig. 2. The vibrations of H_2O are at around 1633 cm^{-1}. The features around 1081 cm^{-1} and 959 cm^{-1} indicate Si–O–Si and Si–O–H stretching vibrations, respectively. The bands around 797 cm^{-1} and 466 cm^{-1} result from Si–O–Si vibrations. The spectra of samples show characteristic bands for methene stretching vibrations around 3000–2800 cm^{-1}. The characteristic peaks at around 1550, 1590 and 3435 cm^{-1} for $-NH_2$ are

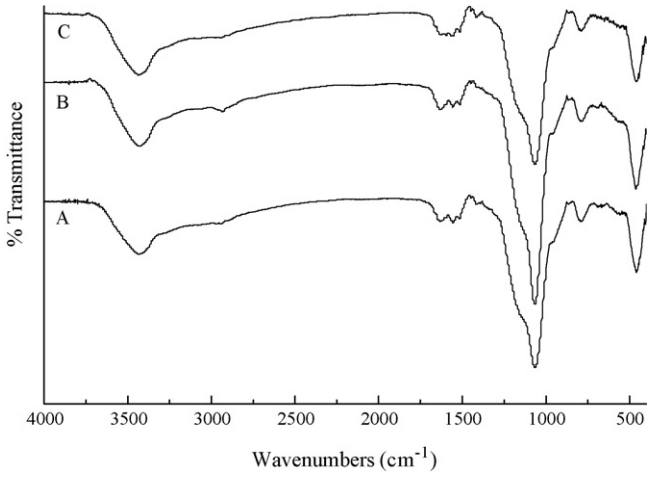

Fig. 2. FTIR spectra of adsorbents A, B and C.

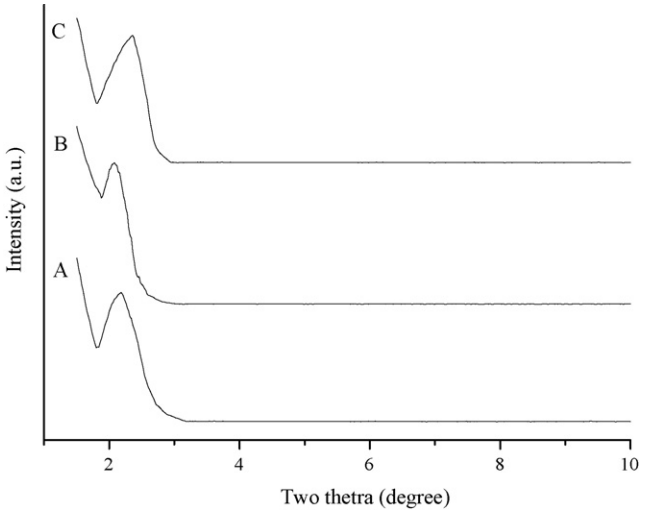

Fig. 3. XRD patterns of adsorbents A, B and C.

also the strong evidence for successful grafting of functional groups [37,38].

The XRD patterns of all the three adsorbents, A, B and C, show a single diffraction peak (1 0 0) at 2.18°, 2.1°and 2.32°of 2θ, respectively (Fig. 3). Although three additional high order peaks (1 1 0, 2 0 0 and 2 1 0) for the modification of amino are absent in Fig. 3, the sharp peak (1 0 0) indicates that the ordered mesostructures of samples has been maintained after fictionalization.

The BET measurement was performed for each sample. Table 1 shows the porosity data. Figs. 4 and 5 show the nitrogen adsorption–desorption isotherms and pore size distributions

Table 1
Structure properties of three adsorbents

Sample	BET surface area (m^2/g)	Pore size (nm)	Pore volume (cm^3/g)
Adsorbent A	336.3	4.6	0.488
Adsorbent B	128.4	2.4	0.279
Adsorbent C	421.9	6.1	0.556

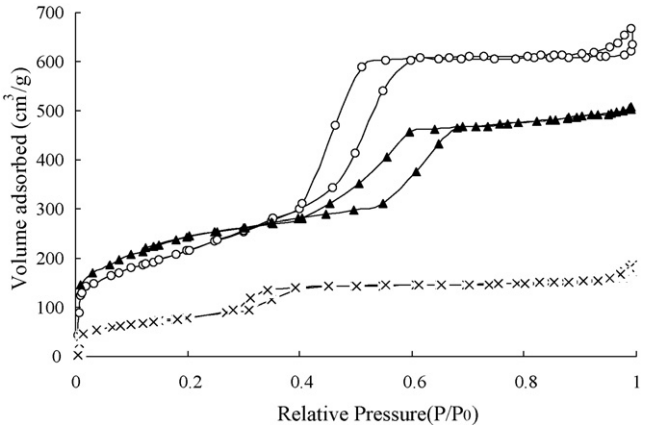

Fig. 4. Nitrogen adsorption–desorption isotherms at 77 K for adsorbents A (▲), B (×) and C (◯).

of three adsorbents, respectively. Fig. 4 reveals that the nitrogen adsorption–desorption isotherms are all in accordance with the type-IV curve, which is the characteristic of mesostructures [2,39]. All samples had narrow pore size distributions (Fig. 5). As expected, adsorbent C, which was synthesized with CTAB and TMAOH as hybrid surfactant templates, exhibited highly enlarged pore, higher BET surface area and pore volume. As a result of the large ionic radius of TMA^+, a relatively weak ion pair was produced for the reaction between TMA^+ and hydroxyl group of hydrolyzed silicates. The ion pair diffused to the surfactant interface and the silicate precursor interacted with surfactant headgroups since the interaction of the silicate precursor with surfactant were stronger than with TMA^+, then the silicates were directed to condensation and polymerization surrounding the surfactant micelles. Thus, TMAOH likely modified the strength of the electrostatic interaction between silicates and the cationic surfactant micelles to promote pore properties [40]. TMAOH helped to accelerate the condensation of silicates and strengthen the physical structure of adsorbent C. Adsorbent B synthesized using CTAB had lower pore size, surface area and pore volume than adsorbent A using P123 since CTAB has a shorter molecular chain than P123. In comparison with adsorbents A and B, the addition of TMAOH enhanced the pore size, surface area and pore volume of adsorbent C.

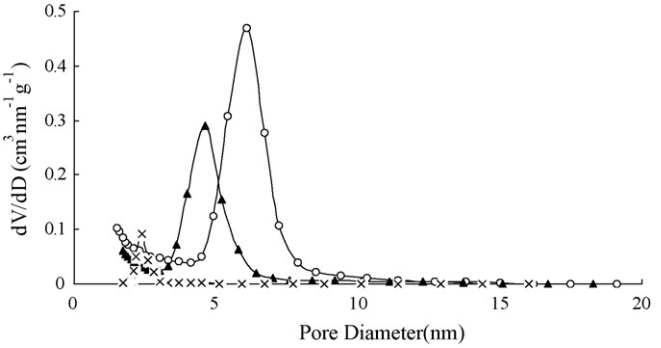

Fig. 5. Pore size distribution curves of adsorbents A (▲), B (×) and C (◯).

Table 2
Cu^{2+} adsorption on three adsorbents

Adsorbent	Cu^{2+} (mmol/L)		Removal (%)	Q (mmol/g)	K_d (mL/g)	Equilibrium pH
	C_0	C_e				
A	1	0.082	91.8	0.1836	2239.02	6.52
B	1	0.371	62.9	0.1258	339.08	5.98
C	1	0.007	99.3	0.1986	28371.43	6.74
A	2	0.688	65.6	0.2624	381.40	5.54
C	2	0.435	78.3	0.3130	719.54	6.03
A	4	2.392	40.2	0.3216	134.45	5.33
C	4	2.048	48.8	0.3904	190.63	5.75

Table 3
Pb^{2+} adsorption on three adsorbents

Adsorbent	Pb^{2+} (mmol/L)		Removal (%)	Q (mmol/g)	K_d (mL/g)	Equilibrium pH
	C_0	C_e				
A	1	0.034	96.6	0.1932	5682.35	6.72
B	1	0.309	69.1	0.1382	447.25	6.02
C	1	0.006	99.4	0.1988	33133.33	6.81
A	2	0.585	70.8	0.2830	483.76	6.21
C	2	0.363	81.9	0.3274	901.93	6.38
A	4	2.292	42.7	0.3416	149.04	5.91
C	4	1.959	51.0	0.4082	208.37	6.07

3.2. Adsorption characteristics of mesoporous adsorbents in metal solutions

The ability of adsorbents to remove a metal ion from aqueous solution can be expressed in terms of the amount of metal ions on the adsorbents (Q) and the distribution ratio (K_d). They can be calculated according to Eqs. (1) and (2):

$$Q = (C_0 - C_e) \times \frac{V}{W} \quad (1)$$

$$K_d = \frac{10^3 Q}{C_e} \quad (2)$$

where Q is the amount of metal ion on the adsorbents (mmol/g), K_d is the distribution ratio of the metal (mL/g), V is the volume of the aqueous solution (L), W is the weight of the adsorbent (g), C_0 (mmol/L) and C_e (mmol/L) are the initial and final concentrations of the given ion in solution.

Tables 2–7 give the adsorption data of Cu^{2+}, Pb^{2+}, Zn^{2+}, Mn^{2+}, Fe^{2+} and Ag^{+}. It was found that adsorbent C possessed higher loading capacity and distribution constant than the other ones. The performance of three adsorbents decreases in the following order: C > A > B. The values of Q and K_d of adsorbent B are much smaller than those of adsorbent A. In contrast, adsorbent C, which used TMAOH as subsidiary structure-directing agent, remarkably improved the ability of metal ions removal and even exceeded adsorbent A. TMAOH was a good mineralizer so as to accelerate aeolotropy during the formation of mesostructure and further pore size and uniform distribution of organic groups. Therefore, the loading capacity of adsorbent C modified with APTES was greater than some reported counterpart [41,42].

The amino hydrolyzation was promoted due to the chelation between amino and metal ions. As a result, at the same ion concentration, the values of equilibrium pH rose with the increase of the ion adsorption quantity. The adsorption approached to a saturation state with the enhancement of the initial concentrations. The higher initial concentrations of metals were used, the lower equilibrium pH values were produced. In addition, the K_d values of adsorbents A, B and C all decreased in the

Table 4
Zn^{2+} adsorption on three adsorbents

Adsorbent	Zn^{2+} (mmol/L)		Removal (%)	Q (mmol/g)	K_d (mL/g)	Equilibrium pH
	C_0	C_e				
A	1	0.127	87.3	0.1746	1374.80	7.04
B	1	0.485	51.5	0.1030	212.37	6.63
C	1	0.049	95.1	0.1902	3881.63	7.15
A	2	0.796	60.2	0.2408	302.51	6.84
C	2	0.513	74.4	0.2974	579.73	6.95
A	4	2.402	40.0	0.3196	133.06	6.56
C	4	2.192	45.2	0.3616	164.96	6.75

Table 5
Mn^{2+} adsorption on three adsorbents

Adsorbent	Mn^{2+} (mmol/L)		Removal (%)	Q (mmol/g)	K_d (mL/g)	Equilibrium pH
	C_0	C_e				
A	1	0.300	70.0	0.1400	466.67	7.81
B	1	0.587	41.3	0.0826	140.72	7.57
C	1	0.118	88.2	0.1764	1494.92	7.92
A	2	1.209	39.6	0.1582	130.85	7.71
C	2	0.841	58.0	0.2318	275.62	7.79
A	4	3.116	22.1	0.1768	56.74	7.58
C	4	2.689	32.8	0.2622	97.51	7.64

Table 6
Fe^{2+} adsorption on three adsorbents

Adsorbent	Fe^{2+} (mmol/L)		Removal (%)	Q (mmol/g)	K_d (mL/g)	Equilibrium pH
	C_0	C_e				
A	1	0.037	96.3	0.1926	5205.41	6.94
B	1	0.327	67.3	0.1346	411.63	6.42
C	1	0.006	99.4	0.1988	33133.33	7.08
A	2	0.617	69.2	0.2766	448.30	6.10
C	2	0.389	80.6	0.3222	828.28	6.53
A	4	2.379	40.5	0.3242	136.28	5.79
C	4	2.007	49.8	0.3986	198.60	6.15

order: $Ag^+ > Pb^{2+} > Fe^{2+} > Cu^{2+} > Zn^{2+} > Mn^{2+}$. It reflected the adsorption selectivity of mesoporous adsorbents modified with amine for metal ions to a certain extent.

3.3. Adsorption kinetics of Cu^{2+} by adsorbent C

The adsorption rate is an important parameter used to image the adsorption process. Many applications, such as wastewater treatment and metal purification, need rapid adsorption rate and short contact time.

The pseudo-first-order and pseudo-second-order kinetic models are commonly used to estimate the rate constants, initial adsorption rates and adsorption capacities of an adsorbent for some adsorbates [43–45]. Two nonlinear models (Eqs. (3) and (4)) have been proved to be more applicable than the linear ones [46]:

$$q_t = q_{eq}(1 - \exp^{-k_1 t}) \quad (3)$$

$$q_t = \frac{k_2 q_{eq}^2 t}{(1 + k_2 q_{eq} t)} \quad (4)$$

where t is the contact time (min); q_t (mmol/g) is the solid-phase loading of metal ions at time t; k_1 (min^{-1}) and k_2 (g/mmol min) are the rate constants of pseudo-first-order and pseudo-second-order adsorption, respectively; q_{eq} (mmol/g) is the adsorption capacity at equilibrium.

Fig. 6 illustrates the kinetic process of Cu^{2+} adsorption onto adsorbent C. During the initial 3 min, the removal efficiency of Cu^{2+} increased to 99.2%, which clearly illuminated that the extraction process of adsorbent C was speeded up in a large scale. By contrasting the values of coefficient of determination (r^2) in Figs. 6A and B, it was found that the pseudo-second-order kinetic model fitted better with kinetic data of adsorbent C than pseudo-first-order kinetic model. The values of q_{eq}, k_2 and $k_2 q_{eq}^2$ (initial adsorption rate) are 0.19876 mmol/g, 827.05469 g/mmol min and 32.67324 mmol/g min, respectively.

Table 7
Ag^+ adsorption on three adsorbents

Adsorbent	Ag^+ (mmol/L)		Removal (%)	Q (mmol/g)	K_d (mL/g)	Equilibrium pH
	C_0	C_e				
A	1	0.019	98.1	0.1962	10326.32	7.69
B	1	0.233	76.7	0.1534	658.37	7.29
C	1	0.001	99.9	0.1998	199800.00	7.82
A	2	0.489	75.6	0.3022	618.00	7.35
C	2	0.293	85.4	0.3414	1165.19	7.54
A	4	2.084	47.9	0.3832	183.88	6.94
C	4	1.852	53.7	0.4296	231.97	7.06

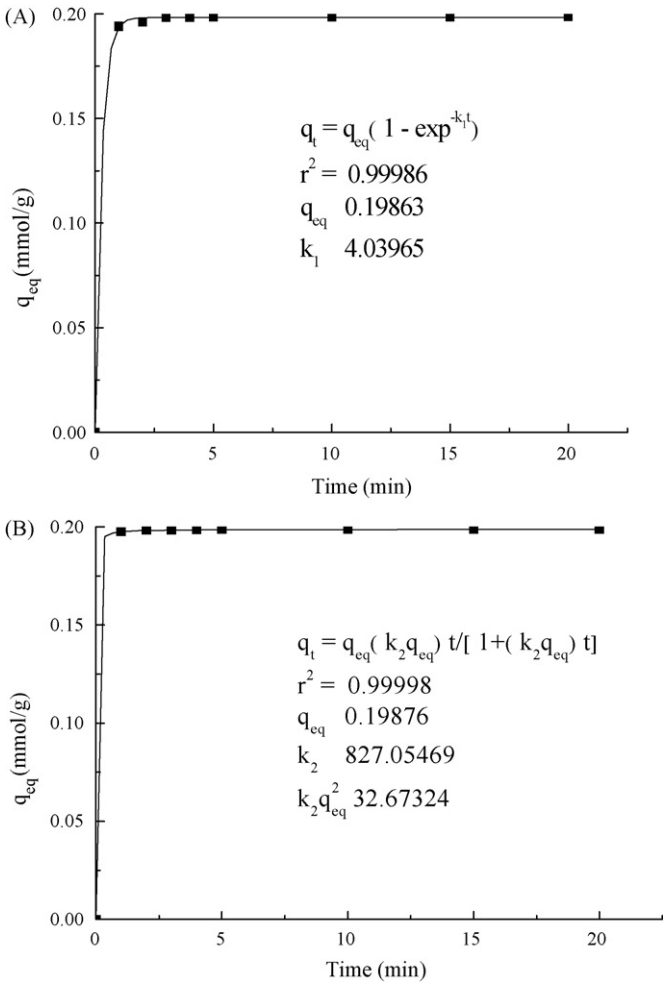

Fig. 6. Pseudo first-order kinetics (A) and pseudo second-order kinetics (B) by nonlinear method for the adsorption of 1 mmol/L Cu^{2+} solution onto adsorbent C.

These data explain the excellent adsorption attribution of adsorbent C again.

3.4. Regeneration of adsorbent C

The same sample of the adsorbent removed over 90% of Cu^{2+} from solutions after eight stripping cycles. Considering the loss of the adsorbent during each cycle, the amount of the adsorbent and the volume of Cu^{2+} solution were adjusted to the comparable measure. Table 8 shows the results of the regeneration process. The adsorption capacity of adsorbent C were maintained at a level more than 0.19 mmol/g and with an uptake ratio more than 94% in the first three cycles. During the following three cycles, the data decreased to 0.184 mmol/g and 92%, respectively. After eight cycles, the loading capacity of adsorbent C reduced to 90.4%. The data showed the excellent regeneration capacity of modified mesoporous adsorbents compared to non-modified ones [47].

Table 8
Eight stripping cycles of adsorbent C

Stripping cycle	W (g)	V (mL)	Removal (%)	Q (mmol/g)	K_d (mL/g)
1	0.100	20	99.5	0.199	39800
2	0.095	19	96.0	0.192	4800
3	0.090	18	94.9	0.190	3725.5
4	0.085	17	93.5	0.187	2876.9
5	0.080	16	93.0	0.186	2657.1
6	0.075	15	92.0	0.184	2300
7	0.070	14	90.0	0.180	1800
8	0.065	13	90.4	0.181	1885.4

3.5. Adsorption isotherm of metal ions by adsorbent C

Langmuir and Freundlich equations are two common isotherm models to describe the behavior of adsorbents and the correlation between adsorption parameters. In this work, the two models were used to test the adsorption process of adsorbent C.

The Langmuir isotherm is expressed as Eq. (5):

$$q_{eq} = bQ_{max}\frac{C_{eq}}{(1 + bC_{eq})} \tag{5}$$

where q_{eq} (mmol/g) is the equilibrium loading capacity of adsorbent, Q_{max} (mmol/g) is the maximum adsorption capacity corresponding to complete monolayer coverage, C_{eq} (mmol/L) is the equilibrium concentration of the adsorbate, and b (L/mmol) is the equilibrium constant related to the adsorption energy.

It can be represented in a linear expression as Eq. (6) [46]:

$$\frac{C_{eq}}{q_{eq}} = \frac{1}{bQ_{max}} + \frac{C_{eq}}{Q_{max}} \tag{6}$$

According to Eq. (6), Q_{max} and b values can be determined experimentally by plotting C_{eq} versus C_{eq}/q_{eq}.

The Freundlich isotherm assumes that different sites are involved with several adsorption energies, so it can be applied to nonideal adsorption on heterogeneous surfaces as well as multilayer adsorption [48,49]. The Freundlich model is described as Eq. (7):

$$q_{eq} = kC_{eq}^{1/n} \tag{7}$$

where k is the Freundlich constant and $1/n$ is the heterogeneity factor.

The linear form can be represented by:

$$\lg q_{eq} = \lg k + (1/n)\lg C_{eq} \tag{8}$$

The constants of the Langmuir isotherm and the Freundlich isotherm are summarized in Tables 9 and 10, respectively.

Table 9
Langmuir isotherm constants for Cu^{2+}, Pb^{2+}, Zn^{2+}, Mn^{2+}, Fe^{2+} and Ag^{+}

Metal ions	b	Q_{max}	r^2
Cu^{2+}	28.9180	0.3939	0.9971
Pb^{2+}	33.7167	0.4119	0.9979
Zn^{2+}	18.0332	0.3682	0.9979
Mn^{2+}	16.4700	0.2662	0.9986
Fe^{2+}	33.2083	0.4020	0.9978
Ag^{+}	42.1350	0.4331	0.9982

Table 10
Freundlich isotherm constants for Cu^{2+}, Pb^{2+}, Zn^{2+}, Mn^{2+}, Fe^{2+} and Ag^{+}

Metal ions	k	$1/n$	r^2
Cu^{2+}	0.3619	0.1483	0.9753
Pb^{2+}	0.3829	0.1497	0.9844
Zn^{2+}	0.3281	0.2128	0.9787
Mn^{2+}	0.2338	0.1762	0.9715
Fe^{2+}	0.3732	0.1461	0.9818
Ag^{+}	0.4075	0.1222	0.9799

Compare the r^2 values in Tables 9 and 10, all experimental data are demonstrated in less accordance with the Freundlich isotherm model than the Langmuir isotherm model. Thus, the adsorption behavior of adsorbent C for the above metal ions mostly belonged to monolayer adsorption. The equilibrium constant (b) and maximum adsorption capacity (Q_{max}) of adsorbent C increased as the following order: $Mn^{2+} < Zn^{2+} < Cu^{2+} < Fe^{2+} < Pb^{2+} < Ag^{+}$.

4. Conclusions

In this work, "One-step" and "EISA" procedure (nontoxic ethanol as solvent) were combined together for the synthesis of mesoporous materials. TMAOH and CTAB were used in combination as hybrid templates to fabricate mesoporous adsorbents. It was found that the synthesized product exhibited better adsorption properties than the counterpart only using the copolymer P123 as the surfactant. This adsorbent had a great adsorption capacity mainly due to the uniform distribution of amine inside channels as well as large and well-proportioned pore size. The order of adsorption capacity for six metal ions in this study was $Mn^{2+} < Zn^{2+} < Cu^{2+} < Fe^{2+} < Pb^{2+} < Ag^{+}$. According to the r^2 values, experimental data followed the Langmuir model of monolayer adsorption.

References

[1] H.J. Im, Y.H. Yang, L.R. Allain, C.E. Barnes, S. Dai, Z.L. Xue, Functionalized sol–gels for selective copper(II) separation, Environ. Sci. Technol. 34 (11) (2000) 2209–2214.

[2] T. Kang, Y. Park, K. Choi, J.S. Lee, J. Yi, Ordered mesoporous silica (SBA-15) derivatized with imidazole-containing functionalities as a selective adsorbent of precious metal ions, J. Mater. Chem. 14 (6) (2004) 1043–1049.

[3] G. Dubois, C. Reye, R.J.P. Corriu, C. Chuit, Organic-inorganic hybrid materials. Preparation and properties of dibenzo-18-crown-6 ether-bridged polysilsesquioxanes, J. Mater. Chem. 10 (5) (2000) 1091–1098.

[4] M.C. Burleigh, S. Dai, E.W. Hagaman, J.S. Lin, Imprinted polysilsesquioxanes for the enhanced recognition of metal ions, Chem. Mater. 13 (8) (2001) 2537–2546.

[5] G.Z. Fang, J. Tan, X.P. Yan, Synthesis and evaluation of an ion-imprinted functionalized sorbent for selective separation of cadmium ion, Sep. Sci. Technol. 40 (8) (2005) 1597–1608.

[6] Q. Wei, Z.R. Nie, Y.L. Hao, Z.X. Chen, J.X. Zou, W. Wang, Direct synthesis of thiol-ligands-functionalized SBA-15: effect of 3-mercaptopropyltrimethoxysilane concentration on pore structure, Mater. Lett. 59 (28) (2005) 3611–3615.

[7] M. Chatterjee, T. Iwasaki, Y. Onodera, H. Hayashi, Y. Ikushima, T. Nagase, T. Ebina, Hydrothermal synthesis and characterization of copper containing crystalline silicate mesoporous materials from gel mixture, Appl. Clay Sci. 25 (3–4) (2004) 195–205.

[8] D.W. Park, S.D. Choi, S.J. Choi, C.Y. Lee, G.J. Kim, Asymmetric epoxidation of styrene on the heterogenized chiral salen complexes prepared from organo-functionalized mesoporous materials, Catal. Lett. 78 (1–4) (2002) 145–151.

[9] Y.D. Lu, M.J. Yuan, Y. Liu, B. Tu, C.H. Xu, B.H. Liu, D.Y. Zhao, J.L. Kong, Photoelectric performance of bacteria photosynthetic proteins entrapped on tailored mesoporous WO_3–TiO_2 films, Langmuir 21 (9) (2005) 4071–4076.

[10] S.P. Naik, W. Fan, T. Yokoi, T. Okubo, Synthesis of a three-dimensional cubic mesoporous silica monolith employing an organic additive through an evaporation-induced self-assembly process, Langmuir 22 (14) (2006) 6391–6397.

[11] J.H. Pan, S.Y. Chai, W.I. Lee, Photocatalytic properties of mesoporous TiO_2 films derived from evaporation-induced self-assembly method, Mater. Sci. Forum 510–511 (2006) 58–61.

[12] M. Etienne, A. Walcarius, Evaporation induced self-assembly of templated silica and organosilica thin films on various electrode surfaces, Electrochem. Commun. 7 (12) (2005) 1449–1456.

[13] P.D. Yang, D.Y. Zhao, D.I. Margolese, B.F. Chmelka, G.D. Stucky, Generalized synthesis of large-pore mesoporous metal oxides with semicrystalline frameworks, Nature 396 (6707) (1998) 152–155.

[14] P.D. Yang, T. Deng, D.Y. Zhao, D. Pine, B.F. Chmelka, G.M. Whitesides, G.D. Stucky, Hierarchically ordered oxides, Science 282 (5397) (1998) 2244–2246.

[15] P.D. Yang, D.Y. Zhao, D.I. Margolese, B.F. Chmelka, G.D. Stucky, Synthesis of continuous mesoporous silica thin films with three-dimensional accessible pore structures, Chem. Commun. 22 (1998) 2499–2500.

[16] D.Y. Zhao, P. Yang, N. Melosh, J.L. Feng, B.F. Chmelka, G.D. Stucky, Continuous mesoporous silica films with highly ordered large pore structures, Adv. Mater. 10 (16) (1998) 1380–1385.

[17] Z.D. Zhang, X.X. Yan, B.Z. Tian, C.Z. Yu, B. Tu, G.S. Zhu, S.L. Qiu, D.Y. Zhao, Synthesis of ordered small pore mesoporous silicates with tailorable pore structures and sizes by polyoxyethylene alkyl amine surfactant, Microporous Mesoporous Mater. 90 (1–3) (2006) 23–31.

[18] M. Etienne, A. Walcarius, Analytical investigation of the chemical reactivity and stability of aminopropyl-grafted silica in aqueous medium, Talanta 59 (6) (2003) 1173–1188.

[19] K. Tajima, L.S. Li, S.I. Stupp, Nanostructured oligo (*p*-phenylene vinylene)/silicate hybrid films: one-step fabrication and energy transfer studies, J. Am. Chem. Soc. 128 (16) (2006) 5488–5495.

[20] K. Yu, A.J. Hurd, A. Eisenberg, C.J. Brinker, Synthesis of silica/polystyrene-block-poly(ethylene oxide) films with regular and reverse mesostructures of large characteristic length scales by solvent evaporation-induced self-assembly, Langmuir 17 (26) (2001) 7961–7965.

[21] L.M. Yang, Y.J. Wang, G.S. Luo, Y.Y. Dai, Functionalization of SBA-15 mesoporous silica with thiol or sulfonic acid groups under the crystallization conditions, Microporous Mesoporous Mater. 84 (1–3) (2005) 275–282.

[22] T. Kang, Y. Park, J. Yi, Highly selective adsorption of Pt^{2+} and Pd^{2+} using thiol-functionalized mesoporous silica, Ind. Eng. Chem. Res. 43 (6) (2004) 1478–1484.

[23] Y.H. Lin, G.E. Fryxell, H. Wu, M. Engelhard, Selective sorption of cesium using self-assembled monolayers on mesoporous supports, Environ. Sci. Technol. 35 (19) (2001) 3962–3966.

[24] J.F. Bardeau, A. Gourbil, M. Dutreilh-Colas, S. Dourdain, A. Mehdi, A. Gibaud, X-ray reflectivity study of acid-base post-synthesis treatments of mesoporous thin films templated by P123, Thin Solid Films 495 (1–2) (2006) 191–196.

[25] M.H. Lim, A. Stein, Comparative studies of grafting and direct syntheses of inorganic-organic hybrid mesoporous materials, Chem. Mater. 11 (11) (1999) 3285–3295.

[26] T. Yokoi, H. Yoshitake, T. Tatsumi, Synthesis of amino-functionalized MCM-41 via direct co-condensation and post-synthesis grafting methods using mono-, di- and tri-amino-organoalkoxysilanes, J. Mater. Chem. 14 (6) (2004) 951–957.

[27] C.M. Yang, Y.Q. Wang, B. Zibrowius, F. Schuth, Formation of cyanide-functionalized SBA-15 and its transformation to carboxylate-functionalized SBA-15, Phys. Chem. Chem. Phys. 6 (9) (2004) 2461–2467.

[28] J. Brown, L. Mercier, T.J. Pinnavaia, Selective adsorption of Hg^{2+} by thiol-functionalized nanoporous silica, Chem. Commun. 1 (1999) 69–70.

[29] D. Margolese, J.A. Melero, S.C. Christiansen, B.F. Chmelka, G.D. Stucky, Direct synthesis of ordered SBA-15 mesoporous silica containing sulfonic acid groups, Chem. Mater. 12 (8) (2000) 2448–2459.
[30] I. Diaz, F. Mohino, J. Perez-Pariente, E. Sastre, Synthesis, characterization and catalytic activity of MCM-41-type mesoporous silicas functionalized with sulfonic acid, Appl. Catal. A Gen. 205 (1–2) (2001) 19–30.
[31] J.Q. Yu, Z.C. Feng, L. Xu, M.J. Li, Q. Xin, Z.M. Liu, C. Li, Ti-MCM-41 synthesized from colloidal silica and titanium trichloride: synthesis, characterization, and catalysis, Chem. Mater. 13 (3) (2001) 994–998.
[32] A. Walcarius, C. Delacote, Rate of access to the binding sites in organically modified silicates. 3. Effect of structure and density of functional groups in mesoporous solids obtained by the co-condensation route, Chem. Mater. 15 (22) (2003) 4181–4192.
[33] C.F. Cheng, W.Z. Zhou, D.H. Park, J. Klinowski, M. Hargreaves, L.F. Gladden, Controlling the channel diameter of the mesoporous molecular sieve MCM-41, J. Chem. Soc. Faraday Trans. 93 (2) (1997) 359–363.
[34] A. Sayari, Unprecedented expansion of the pore size and volume of periodic mesoporous silica, Angew. Chem. Int. Ed. 39 (16) (2000) 2920–2922.
[35] Z. Yan, G.T. Li, L. Mu, S.Y. Tao, Pyriding-functionalized mesoporous silica as efficient adsorbent for the removal of acid dyestuffs, J. Mater. Chem. 16 (18) (2006) 1717–1725.
[36] Y.K. Lu, X.P. Yan, An imprinted organic-inorganic hybrid sorbent for selective separation of cadium from aqueous solution, Anal. Chem. 76 (2) (2004) 453–457.
[37] D. Lin-Vien, N.B. Colthup, W.G. Fately, J.G. Grasselli, The Handbook of Infrared and Raman Characteristic Frequencies of Organic Molecules, Academic Press, London, 1991.
[38] K.Y. Ho, G. McKay, K.L. Yeung, Selective adsorbents from ordered mesoporous silica, Langmuir 19 (7) (2003) 3019–3024.
[39] M. Kruk, M. Jaroniec, A. Sayari, A unified interpretation of high-temperature pore size expansion processes in MCM-41 mesoporous silicas, J. Phys. Chem. B 103 (22) (1999) 4590–4598.
[40] Z.H. Luan, D.Y. Zhao, H.Y. He, J. Klinomski, L. Kevan, Characterization of aluminophosphate-based tubular mesoporous molecular sieves, J. Phys. Chem. B 102 (7) (1998) 1250–1259.
[41] M. Takafuji, S. Ide, H. Ihara, Z.H. Xu, Preparation of poly(1-vinylimidazole)-grafted magnetic nanoparticles and their application for removal of metal ions, Chem. Mater. 16 (10) (2004) 1977–1983.
[42] L. Bois, A. Bonhomme, A. Ribes, B. Pais, G. Raffin, F. Tessier, Functionalized silica for heavy metal ions adsorption, Colloid. Surf. Physicochem. Eng. Aspect. 221 (1–3) (2003) 221–230.
[43] M. Ozacar, I.A. Sengil, A two stage batch adsorber design for methylene blue removal to minimize contact time, J. Environ. Manage. 80 (4) (2006) 372–379.
[44] W. Rudzinski, W. Plazinski, Kinetics of solute adsorption at solid/solution interfaces: a theoretical development of the empirical pseudo-first and pseudo-second order kinetic rate equations, based on applying the statistical rate theory of interfacial transport, J. Phys. Chem. B 110 (33) (2006) 16514–16525.
[45] Y.S. Ho, G. McKay, Sorption of dye from aqueous solution by peat, Chem. Eng. J. 70 (2) (1998) 115–124.
[46] K.V. Kumar, Linear and non-linear regression analysis for the sorption kinetics of methylene blue onto activated carbon, J. Hazard. Mater. 137 (3) (2006) 1538–1544.
[47] A. Sayari, S. Hamoudi, Y. Yang, Applications of pore-expanded mesoporous silica. 1. Removal of heavy metal cations and organic pollutants from wastewater, Chem. Mater. 17 (1) (2005) 212–216.
[48] B.C. Pan, Y. Xiong, A.M. Li, J.L. Chen, Q.X. Zhang, X.Y. Jin, Adsorption of aromatic acids on an aminated hypercrosslinked macroporous polymer, React. Funct. Polym. 53 (2–3) (2002) 63–72.
[49] Z. Reddad, C. Gerente, Y. Andres, P.L. Cloirec, Adsorption of several metal ions onto a low-cost biosorbent: kinetic and equilibrium studies, Environ. Sci. Technol. 36 (9) (2002) 2067–2073.